Microstructural Analysis Of Unidirectional Composites
A Comparison Of Data Reduction Schemes

Yuksel, O.; Hartley, R.; Broggi, G.; Maes, V.; Gomarasca, S.; Baumard, T.; Reun, A.L.; Dransfeld, C.; Caglar, B.; More Authors

Publication date
2024

Document Version
Final published version

Published in
Proceedings of the 21st European Conference on Composite Materials

MICROSTRUCTURAL ANALYSIS OF UNIDIRECTIONAL COMPOSITES: A COMPARISON OF DATA REDUCTION SCHEMES

O. Yuksel[1], R. Hartley[2], G. Broggi[1], V. Maes[2], S. Gomarasca[1], T. Baumard[3], A.L. Reun[3], A. Levy[3], C. Dransfeld[1], B. Caglar[1] and J. Kratz[2]

[1]Aerospace Structures and Materials Department, Faculty of Aerospace Engineering, Delft University of Technology, Delft, the Netherlands
Email adresses : o.yuksel@tudelft.nl, g.broggi@tudelft.nl, s.gomarasca@tudelft.nl, c.a.dransfeld@tudelft.nl, b.caglar@tudelft.nl,
[2]Bristol Composites Institute, University of Bristol, Queen's Building, University Walk, Bristol, BS8 1TR, United Kingdom
Email adresses : robin.hartley@bristol.ac.uk, vincent.maes@bristol.ac.uk, james.kratz@bristol.ac.uk
[3]Nantes Université, IRT Jules Verne, CNRS, Laboratoire de thermique et énergie de Nantes, LTeN, UMR 6607, F-44000 Nantes, France
Email adresses : theo.baumard@univ-nantes.fr, adrien.le-reun@univ-nantes.fr, arthur.levy@univ-nantes.fr

Keywords: Micrograph, Microstructure, Image analysis

Abstract
This study presents the first steps of a benchmarking exercise on image processing of composite materials. Employing three distinct imaging protocols and five different image processing algorithms, the research explains the variability in capturing microstructural features of common micrograph dataset. Results highlight the sensitivity of different methods to factors like illumination inhomogeneities and pixel density, influencing the accuracy and consistency of obtained results. By comparing methodologies from different researchers in a blind format, the study identifies strengths and limitations, laying the groundwork for future benchmarking activities. Moving forward, this research sets the stage for standardized protocols and guidelines, aiming to enhance the reproducibility and reliability of microstructural analysis in composite materials. Such efforts are crucial for advancing material design and development, ultimately creating tailored composite materials with enhanced performance and functionality.

1. Introduction

Composite laminates have long been described using homogenized quantities such as fiber volume fraction (V_f), ply thickness, void content or fiber orientation. While these lumped scalar quantities offer valuable insights into material properties, they fall short of fully characterizing micro- and meso-structural features thus limiting the predictive capabilities of manufacturing and structural behavior at the local level. Consequently, the composites community is increasingly turning its attention to micro- and mesoscale analyses of composite materials. Recent studies have showcased the superior predictive capabilities of this approach compared to lumped material properties [1,2]. Various features, including porosity [3], local fiber distribution and orientation, ply thickness, or yarn geometry, significantly influence properties like permeability [4] or strength [5,6].

Micrographical and tomographical analyses constitute the primary experimental techniques for microstructural assessment. Both approaches necessitate image-based analysis tools, whether in 2D or 3D. With growing interest in micro- and meso-structural descriptors and advancements in hardware and software capabilities for acquisition and processing, this field has witnessed significant developments in recent decades. However, there has been limited effort devoted to quantifying the comparative

performances of algorithms, establishing guidelines to enhance consistency between researchers, and supporting early-stage researchers in ensuring accurate microstructure analysis.

This work addresses these gaps by capturing three micrographs using a confocal scanning microscope from the same polished sample, following three distinct protocols representative of techniques used by the composites community . Multiple images were acquired to scan a cross-sectional area ranging from 2 mm to 3.8 mm, using three different objectives to obtain varying pixel densities and illumination. Subsequently, the micrographs were analyzed at the University of Bristol, Nantes Université, and the Technical University of Delft in a blind format using in-house algorithms and methods. The resultant datasets were compared using various statistical analyses to comprehend the variability in the captured microstructures. These findings are discussed comprehensively, laying the groundwork for future benchmarking activities.

2. Methodology

2.1 Sample manufacturing

The composite laminate analyzed in this study was fabricated using a T700G fiber-reinforced low-melt polyaryl ether ketone (LM-PAEK) unidirectional prepreg system (TC1225; Toray Advanced Composites, United States). The prepreg, supplied in 12-inch rolls, consisted of 16 layers of 30 cm-long pieces stacked in a unidirectional sequence. Consolidation was conducted using a hot press (JOOS Press, United States), heating to 380 °C at a rate of 2 °C/min, holding at temperature for 30 mins, then cooling to room temperature at a rate of 2 °C/min, with a consolidation pressure of 10 MPa.

The analyzed sample was extracted from the middle section of the laminate, embedded in clear epoxy, and ground using grinding papers ranging from FEPA 500 to FEPA 4000 with a Struers polishing machine. Subsequent polishing utilized two different ‘DUR’ polishing cloths with 3 µm and 1 µm particle-sized diamond suspensions

2.2. Image acquisition

A Keyence VK-X1000 confocal microscope was employed to capture images. A cross-sectional area of 3.8 mm by 2 mm was scanned by taking successive pictures, or subframes, over a regular grid. The pictures were then stitched using the image stitching plugin in Fiji [7]. Three distinctive acquisition conditions were achieved using three different objectives with the same polished cross-sectional area. The first micrograph was captured using an objective with a working distance of 1.1 mm, providing a 50x magnification. The second micrograph utilized an objective (Plan) offering 20x magnification with a working distance of 3.1 mm. The third micrograph employed an objective (ELWD) with an extra-long working distance of 11.0 mm, also providing 20x magnification. The higher magnification image boasted a pixel density of 3615 pixels/mm, while the others had a pixel density of 1446 pixels/mm. Each micrograph exhibited distinct features such as contrast differences between resin and fibers, grayscale intensities of fibers’ cross-sections, and illumination inhomogeneities. These micrographs and arbitrarily chosen zoomed-in sections are shown in Figure 1.

2.3. Image processing

In this preliminary edition of a benchmarking exercise on image processing of composite materials, five different methods from researchers at three different institutes were applied to the corresponding images. The results were anonymized and presented with participant numbers from #1 to #5, randomly assigned to different algorithms/methods. The participants reported the fiber coordinates and radii that were then further analyzed using the same methodology.

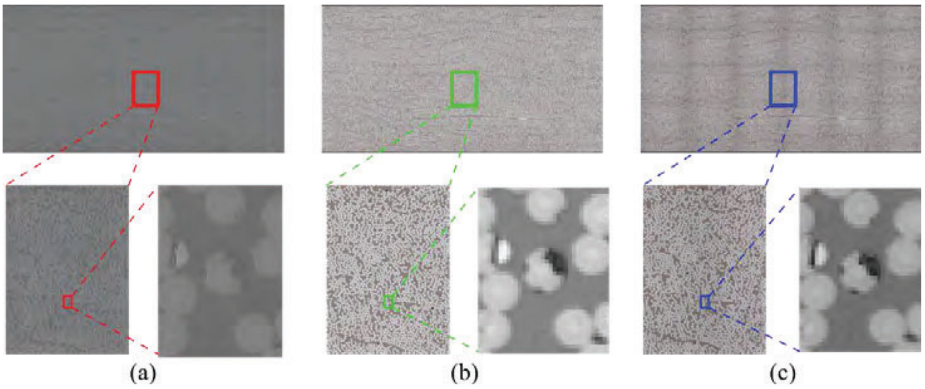

Figure 1. The complete micrographs and the zoomed-in snippets from (a) the 50x magnification image, (b) the 20x magnification image taken by the 'Plan' objective, and (c) the 20x magnification image taken by the 'ELWD' objective.

3. Results and Discussion

Micrograph processing algorithms are intended to extract microstructural characteristics, such as the overall fiber volume fraction or average fiber radius. Table 1 reports these estimated values for the considered cross-section. The estimated fiber volume fraction ranged from 0.45 to 0.65. Fiber volume fraction is computed as the total area of fibers (sum of pi*r^2) divided to the total area of the image and hence potentially could be calculated above 1. Note that the cross-section was large enough for edge effects to be negligible, meaning that the scattering reported is due to differences in fiber analysis. While the 50X magnification image showed better agreement with a coefficient of variation (CoV) of 5.7%, it was 10.6% and 12.3% for the 20X magnification images. Some methods estimated lower fiber volume fraction values for 20X magnification images, while others estimated higher values. Fiber counts were mostly stable across participants, with only a slight variation observed for one method. Average detected fiber radius values ranged from 3.1 µm to 3.7 µm, with corresponding CoVs of 2.8%, 5.3%, and 6.0% for the 50X, 20X (Plan), and 20X (ELWD) images.

Table 1. Estimated fiber volume fraction, fiber count, and average radius values (in micrometer in parentheses).

	Fiber volume ratio			Detected fiber count			Average radius [pixels (µm)]		
	50X	20X (Plan)	20X (ELWD)	50X	20X (Plan)	20X (ELWD)	50X	20X (Plan)	20X (ELWD)
Participant #1	0.56	0.54	0.54	113455	113245	113145	12.42 (3.44)	4.91 (3.40)	4.87 (3.37)
Participant #2	0.52	0.45	0.46	112791	113340	113317	11.95 (3.31)	4.48 (3.10)	4.47 (3.09)
Participant #3	0.60	0.62	0.65	112820	113070	113623	12.81 (3.54)	5.26 (3.64)	5.34 (3.69)
Participant #4	0.57	0.51	0.50	113546	111931	111520	12.46 (3.45)	4.76 (3.29)	4.72 (3.26)
Participant #5	0.51	0.51	0.51	113219	113436	113231	11.88 (3.29)	4.75 (3.29)	4.75 (3.29)
Average	0.55	0.53	0.53	-	-	-	12.30 (3.40)	4.83 (3.34)	4.83 (3.34)
CoV	0.06	0.11	0.12	-	-	-	0.03	0.05	0.06

The spatial distribution of microstructural features also provides valuable insights into the processing-structure-performance relationship for composite materials. In this study, we used the spatial distribution of fiber volume fraction to assess different participants' results and find the root causes of these differences. Figure 2 shows the fiber volume fraction values within 50 by 50 subframes throughout the

cross-section for the 50X image. Overall, each participant's method captured the contrast in fiber volume fraction between the cross-section's relatively high and low-packed regions, a characteristic of a dual-scale composite microstructure. While the first and fourth participant's results were similar, the second and the fifth participants estimated overall lower V_f values, and the third participant estimated higher V_f values, in general.

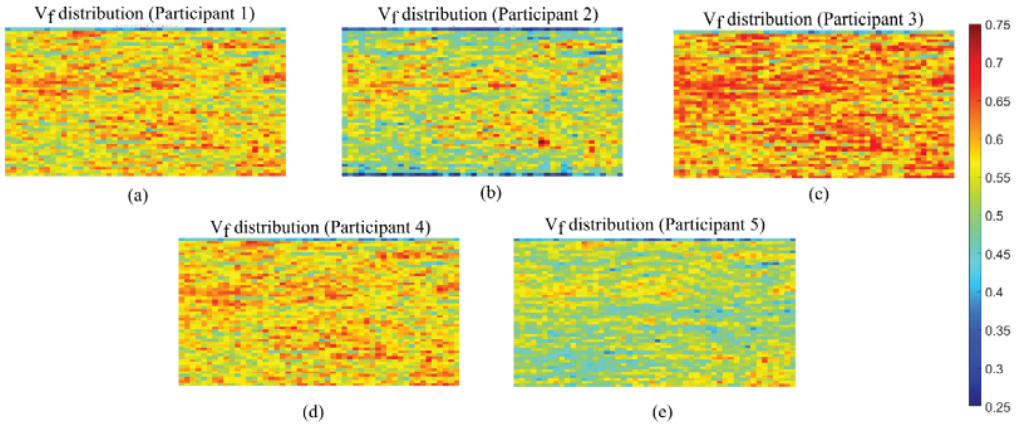

Figure 2. The fiber volume fraction distribution within 50 by 50 subframes throughout the cross-section for the 50X image: (a) Participant #1, (b) Participant #2, (c) Participant #3, (d) Participant #4, (e) Participant #5.

As shown in Figure 1, each micrograph exhibits specific characteristics, such as illumination, that can influence the spatial distribution, especially the boundaries, of the reported microstructural features. The average V_f, radius, and detected fiber counts within the vertical slices over the horizontal axis were plotted in Figure 3. The schematic representation of the vertical slices can be seen in Figure 3 (d). Estimated V_f and radius variation through the horizontal axis reveals that some of the methods were more sensitive to illumination inhomogeneities than others. Stitching boundaries for the 50X and 20X (ELWD) images can be seen in Figure 1, while the 20X (Plan) image does not have apparent stitching boundaries. Especially for the 20X (ELWD) image, the resultant V_f curves of the 2nd and the 3rd methods show high variation, where the valleys on the curves correspond to the shady regions along the stitching boundaries. This influence can also be seen in the results of these participants for the 50X image in a limited manner. These V_f curves were significantly influenced by the estimated average radius values, which decreased around the stitching boundaries. The estimated average radius values for these participants differed for the 50X and 20X(Plan) as well, so the pixel density, the contrast, or the grayscale density are influential parameters for these methods. The 1st and 5th methods seem to provide the most consistent results within three different micrographs, noting that the 5th method assumed to have a uniform radius value throughout the cross-section.

Another essential function of image processing for composite analysis is to extract statistical descriptors that can later be used to generate realistic virtual microstructures. [8,9,10]. Figure 4 reports the distributions of estimated radius values and local Voronoi cell fiber volume fractions for each method and each micrograph. The distributions of radius values get wider in general for the lower magnification images. Local fiber volume fraction distributions were calculated based on the Voronoi cells, the closest fiber to any points within those cells is the corresponding fiber of each cell. Trends in the local fiber volume fraction distributions were similar to the radius distributions. They can be considered as in good agreement for the 50X image. For the 20X images, though, some of the methods tend to estimate higher

or lower radius and local fiber fractions with higher scatter, i.e., wider distributions. On the other hand, the 5th method, using one uniform radius value, shows the most consistent behavior for all the images.

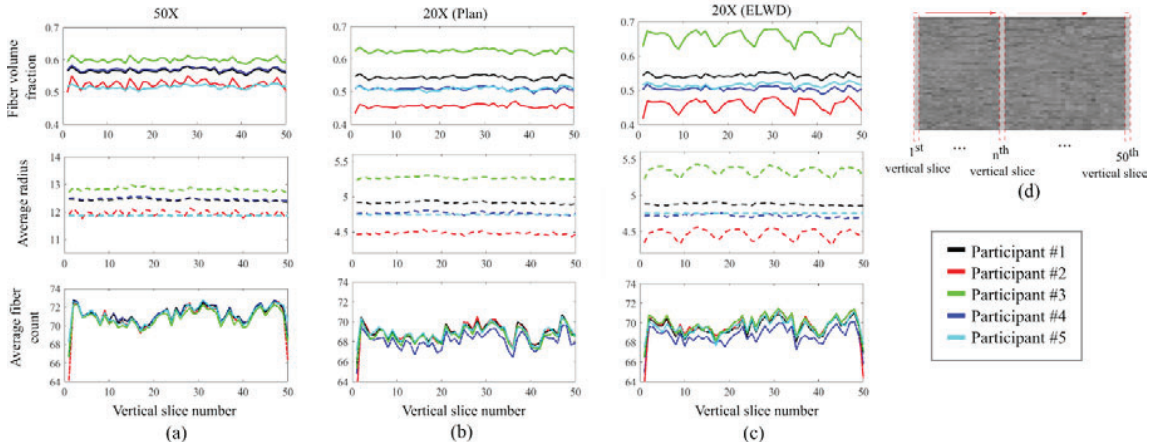

Figure 3. The spatial variation of fiber volume fraction, average fiber radius (in pixels), and average fiber count over the horizontal axis for (a) the 50X image, (b) the 20x (plan) image, and (c) the 20X (ELWD) image. Average values are calculated over a moving vertical window (d).

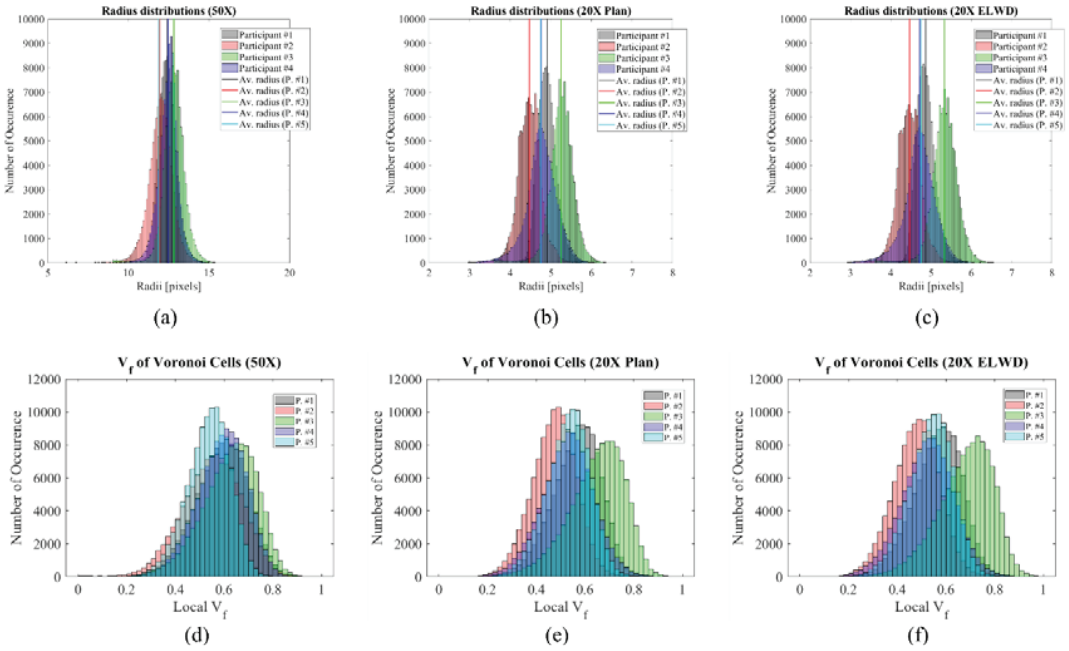

Figure 4. The estimated radius values distributions for (a) 50X, (b) 20X (Plan), and (c) 20X (ELWD) images (bin sizes are 0.1 and 0.04, respectively, for 50X and 20X images). The local fiber volume fraction distributions for, (a) 50X, (b) 20X (Plan), (c) 20X (ELWD) images (bin size is 0.02).

Another important statistical parameter is the neighbor fiber distance. The distribution of neighbor fiber distances provides essential information about composite materials' processing and mechanical performance, such as permeability, a critical property for flow behavior, and failure initiation, which is

strongly dependent on local inhomogeneities. Figure 5 presents the nearest neighbor fiber distance distributions derived from the results of the analyzed algorithms. In agreement with the previously shown distributions, nearest neighbor fiber distributions have a lower scatter for the 50X image compared to the lower magnification images, except for the 5th method. The 5th participant's results show consistent distributions for all images. This observation can be attributed to the uniform fiber radius assumption. Except the 4th method, the results show Gaussian-like distributions with low skewness. The 4th participant seemed to apply a modification step in the image processing algorithm to avoid overlapping fibers which resulted in an artificial peak for the almost touching fiber count. For the 1st participant, a small section of the tail of the distribution is on the negative side. A similar trend can also be seen for the 2nd participant's 50X image results, while this method avoided overlapping fibers but estimated relatively longer distances of the nearest neighbor fibers for the 20X magnification images. For the 3rd participant, the majority of the fibers are overlapping, which explains, in junction with the fiber radius being the highest for this participant, why the computed V_f is highest for Participant 3.

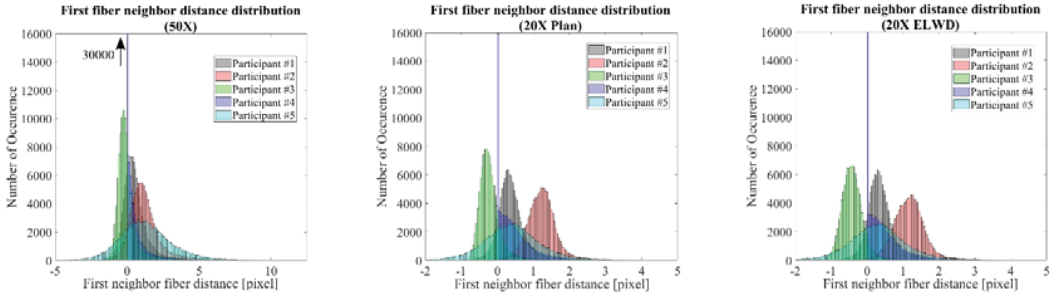

Figure 5. The nearest neighbor fiber distance distributions for (a) 50X, (b) 20X (Plan), and (c) 20X (ELWD) images (bin sizes are 0.1 and 0.04, respectively, for 50X and 20X images).

Although successive polishing operations can achieve a near-perfect sample surface, surface defects on the fiber cross-sections are inevitable in practice. These defects significantly influence the image processing algorithms. Figure 6 shows arbitrarily chosen windows from the same location of the investigated images with the detected fiber locations for each participant. Some of the detected fibers are pointed out within red dashed rectangles in Figure 6. With qualitative visual observation, the precision of the detected fiber locations and radius for 50X magnification is higher compared to the lower magnification images. A deeper analysis of the correlation between the location precision and the surface defects on the corresponding fibers are suggested for the next steps of this benchmarking effort, which would provide valuable information to minimize the influence on the image processing results.

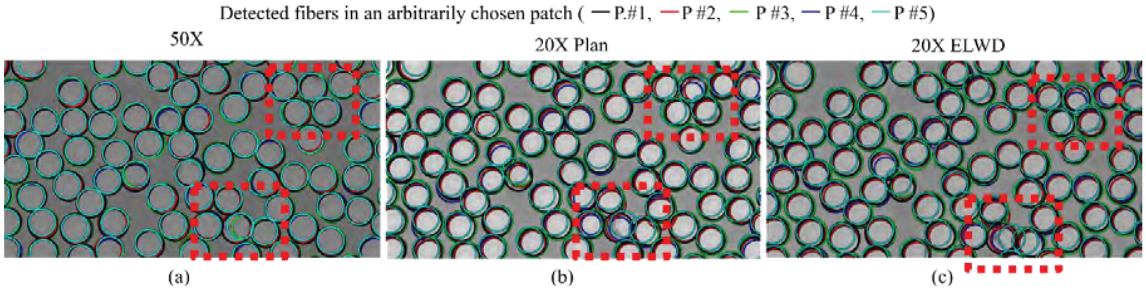

Figure 6. Detected fibers in an arbitrarily chosen window for (a) 50X, (b) 20X (Plan), and (c) 20X (ELWD) images.

4. Conclusions

In conclusion, this study sheds light on the intricacies involved in the microstructural analysis of composite materials, emphasizing the significance of understanding and quantifying the nuances within the image processing algorithms. By employing three distinct imaging protocols and employing various image processing algorithms, this research demonstrates that the choice of processing algorithms and image acquisition conditions significantly influence the obtained microstructural descriptors. However, these parameters are too often overlooked in studies, which raises the question of reproducibility and highlights the need for guidelines defined by the composite community.

Moreover, the comparison of methodologies from different institutions provides valuable insights into the strengths and limitations of each approach, laying the groundwork for future benchmarking endeavors. By anonymizing the results and employing a blind format analysis, this study ensures impartial evaluation and facilitates the identification of potential biases or discrepancies among methodologies.

Moving forward, this research sets the stage for comprehensive benchmarking activities aimed at establishing standardized protocols and guidelines for microstructural analysis in composite materials. Such endeavors are crucial not only for enhancing the reproducibility and reliability of research findings but also for fostering collaboration and knowledge exchange within the composite materials community. Ultimately, by advancing our understanding of microstructural characterization, we can pave the way for the development of tailored composite materials with enhanced performance and functionality.

References

[1] C. Breite, A. Melnikov, A. Turon, A. B. de Morais, C. le Bourlot, E. Maire, E. Schöberl, F. Otero, F. Mesquita, I. Sinclair, J. Costa, J. A. Mayugo, J. M. Guerrero, L. Gorbatikh, L. N. McCartney, M. Hajikazemi, M. Mehdikhani, M. N. Mavrogordato, P. P. Camanho, … Y. Swolfs. Detailed experimental validation and benchmarking of six models for longitudinal tensile failure of unidirectional composites. *Composite Structures*, 279, 2022.

[2] B. Caglar, G. Broggi, M. A. Ali, L. Orgéas, V. Michaud. Deep learning accelerated prediction of the permeability of fibrous microstructures. *Composites Part A: Applied Science and Manufacturing*, 158, 2022.

[3] J. Kratz, P. Galvez-Hernandez, L. R. Pickard, J. Belnoue, K. Potter. Lab-based in-situ micro-CT observation of gaps in prepreg laminates during consolidation and cure. *Composites Part A: Applied Science and Manufacturing*, 140, 2021.

[4] O. Yuksel, B. Caglar, G. Broggi, V. Michaud, R. Akkerman, I. Baran. Saturated transverse permeability of unidirectional rovings for pultrusion: The effect of microstructural evolution through compaction. *Polymer Composites,*45(7): 5935-5952, 2024.

[5] H. Ghayoor, C. C. Marsden, S. v. Hoa, A. R. Melro. Numerical analysis of resin-rich areas and their effects on failure initiation of composites. *Composites Part A: Applied Science and Manufacturing,* 117: 125–133, 2019.

[6] L. Zhuang, A. Pupurs, J. Varna, R. Talreja, Z. Ayadi. Effects of inter-fiber spacing on fiber-matrix debond crack growth in unidirectional composites under transverse loading. *Composites Part A: Applied Science and Manufacturing*, 109: 463–471, 2018.

[7] S. Preibisch, S. Saalfeld, P. Tomancak. Globally optimal stitching of tiled 3D microscopic image acquisitions. *Bioinformatics*, 25(11): 1463–1465, 2009.

[8] J. F. Husseini, E. J. Pineda, S. E. Stapleton. Generation of artificial 2-D fiber reinforced composite microstructures with statistically equivalent features. *Composites Part A: Applied Science and Manufacturing*, 164: 107260, 2023.

[9] Y. Ding, P. P. Camanho, A. Silva. Comparison of three algorithms generating virtual microstructures in terms of the degree of randomness. *Composites Part A: Applied Science and Manufacturing*, 177: 107959, 2024.
[10] R. Guo, M. Alves, M. Mehdikhani, C. Breite, Y. Swolfs. Synthesising realistic 2D microstructures of unidirectional fibre-reinforced composites with a generative adversarial network. *Composites Science and Technology*, 250, 2024.